Research Article

Journal of Environmental Nanotechnology

# ZnSnS Nanoparticles Synthesized by Simple SMI Technique for Photocatalytic Application

K. Valliyammal* and R. Sakthi Sudar Saravanan
Physics Research Centre, Chikkanna Government Arts College, TN, India
Received: 16.07.2024 Accepted: 15.09.2024 Published: 30.09.2024
*nithy.n@gmail.com

## ABSTRACT

Photocatalysis, driven by semiconductor nanoparticles under visible or ultraviolet light, has emerged as a powerful and sustainable approach for environmental remediation and clean energy production. In this study, we investigate the photocatalytic potential of tin (0, 2, 4, 6, 8, 10) mole % alloyed with zinc sulfide (ZnSnS) nanoparticles as efficient catalysts for various environment and energy-related applications. ZnSnS nanoparticles were produced via a simple microwave irradiation technique. Comprehensive structural characterization through X-ray diffraction (XRD), FESEM, EDAX and HRTEM confirmed the successful incorporation of tin atoms into the ZnS crystal lattice. Optical study indicated significant blue shifts in the absorption edge, extending the light absorption into the visible region, a key advantage for photocatalytic applications. Photocatalytic experiments were conducted to evaluate the performance of Zn-alloyed SnS nanoparticles in degrading organic pollutants and hydrogen evolution from water splitting reactions. Our results revealed remarkable enhancements in photocatalytic activity. The enhanced efficiency can be credited to the creation of fresh energy levels within the bandgap, aiding in the separation and movement of charges, and also to the heightened light absorption caused by the reduced bandgap. Furthermore, stability tests indicated the durability of (ZnSnS) nanoparticles, making them suitable candidates for long-term applications in real-world environments. The observed photocatalytic activity enhancements hold promise for addressing environmental issues, including wastewater treatment, air purification, and hydrogen production for clean energy.

**Keywords:** Photocatalyst; Nanoparticles; Solvothermal microwave irradiation technique; Dye.

## 1. INTRODUCTION

In recent years, nanotechnology has become a groundbreaking technology that has revolutionized various industries, altering the characteristics of fundamental materials through manipulation at the atomic level (Nasrollahzadeh *et al.* 2019). This transformation has brought significant changes across various sectors, including medicine and electronics. At the nanoscale, insulating materials can be made to behave like conductors, such as silicon. Certain materials like gold can transition from a solid state to a liquid state at room temperature. These significant changes are solely attributed to nanotechnology. Nanomaterials play a crucial role in removing toxins from the environment. Managing and eliminating environmental pollution has become a significant challenge today. Introducing toxic substances into the water from textile, leather, and paper factories profoundly affects living organisms (Juan *et al.* 2020). Human health is affected by environmental pollution caused by azo dyes such as malachite green (MG), resulting in conditions like skin diseases, allergies, etc. (Mehra *et al*. 2021).

As a result, scientists are exploring new multidisciplinary materials using nanotechnology to address this critical situation. Zinc sulfide (ZnS) exhibits a direct bandgap in two distinct structures. The bandgap of the cubic structure is approximately 3.5- 3.7 eV, while that of the wurtzite structure is 3.7-3.8 eV. ZnS demonstrates high thermal stability, is non-toxic, and its ability to readily accept dopants makes it suitable for various applications in optoelectronic devices, photocatalyst, UV detectors, gas sensors, etc. Researchers are currently concentrating on combining metal ions with ZnS to adjust the optical bandgap of the basic materials (Xu *et al*. 2018). Additionally, ZnS acts as a hindrance to the combination of electron-hole pairs. ZnS has been alloyed with various metal ions such as Sn, Cu, Fe, Cr, Pb, etc. (Tong *et al*. 2023).

Pure ZnS nanomaterials do not show high photocatalytic activity because of their high bandgap value. Notably, the bandgap value of ZnS nanomaterials decreases when alloyed with Sn compared to pure ZnS, indicating the successful insertion of energy levels of alloy into the host ZnS energy band (Gowdhaman *et al*. 2018). This bandgap tuning enhances the photon absorption in the visible region, thereby significantly increasing the photocatalytic activity of ZnS nanomaterials (Yin *et al*. 2016; Rajabi *et al*. 2015; Sharma *et al*. 2021). By varying the alloy's composition, one can attain characteristics between the two end binary components, SnS and ZnS. ZnS nanoparticles are prepared by various physical and chemical methods such

as Co-precipitation (Kripal *et al*. 2010; Hammad *et al*. 2015), hydrothermal (Sabaghi *et al*. 2018), vacuum evaporation technique (Velumani and Ascencio, 2004), electrode deposition (Zhou *et al*. 2013), Microwave assisted co-precipitation (Sonawane *et al*. 2024) etc., There is extensive research on both doped and undoped ZnS nanoparticles. As far as I am aware, there are no reports of a study on Sn alloyed with ZnS nanoparticles. Considering the challenges in forming the alloy, we intend to use a cost-effective Solvothermal Microwave Irradiation (SMI) technique (Gowdhaman *et al*. 2021) to synthesize Sn-alloyed ZnS at concentrations of 0, 0.02, 0.04, 0.06, 0.08, and 0.1M. As a solvent, ethylene glycol helps reduce particle size and promote the formation of a uniform distribution of particles, thereby optimizing the optical characteristics of the nanoparticles reported by (Saravanan *et al*. 2012). The SMI method was employed to produce a large quantity of ZnSnS nanoparticles. The nanoparticles synthesized underwent characterization using XRD, FESEM, and HRTEM to analyze their structural characteristics. EDAX revealed the elements present in the sample, and optical properties were investigated through UV absorption spectra. The attributes of ZnS nanoparticles with Sn alloy show that these particles are effective photocatalysts for breaking down water pollutants.

## 2. EXPERIMENTAL METHOD

Zinc (II) acetate dihydrate $(CH_3COO)_2Zn\cdot 2H_2O$) is likely used as a source of zinc ions ($Zn^{2+}$) in the synthesis process. Zinc ions are a crucial component for forming the $Zn_{1-x}Sn_xS$ nanoparticles. Tin (II) chloride is the tin ions ($Sn^{2+}$) source for creating the $Zn_{1-x}Sn_xS$ nanoparticles. The presence of tin ions is crucial in regulating the composition of the nanoparticles. Thiourea ($CH_4N_2S$) is commonly utilized as a source of sulfur in producing metal sulfide nanoparticles, which contribute to the formation of the sulfide phase in the nanoparticles, including $Zn_{1-x}Sn_xS$. Ethylene Glycol ($C_2H_6O_2$) is a common solvent in various chemical processes, including nanoparticle synthesis. It may be used as a reaction medium or solvent to facilitate the reaction and control particle size and morphology.

The synthesis of Zn alloyed SnS nanoparticles likely involves a combination of these chemicals, along with a well-defined synthesis method, to control the composition and properties of the resulting nanoparticles. The exact procedure and conditions for synthesizing these nanoparticles depend on our specific research or application goals. Additionally, the choice of precursor chemicals and reaction conditions will influence the nanoparticles' characteristics. Start by dissolving 0.1 M of zinc (II) acetate dihydrate and 0.02 M of tin (II) chloride dihydrate in 100 ml of ethylene glycol. Stir this solution at room temperature for 30 minutes. Dissolve 0.3 M of thiourea in a separate container of 100 ml of ethylene glycol at ambient temperature. Gradually incorporate the thiourea solution into the existing solution containing zinc and tin compounds, ensuring continuous agitation. To have a uniform solution, agitating the mixture for an extra hour at room temperature is necessary. Pour the resulting homogeneous solution, which should have a volume of around 200 ml, into a microwave-safe bowl with double walls. Place this bowl in a microwave oven commonly found in households and heat it until the solvent evaporates completely, creating a colloidal precipitate. Allow the colloidal particles to reach room temperature without any external interference naturally. The residue should be thoroughly cleansed using double-distilled water and acetone to remove any remaining impurities and unreacted precursor compounds. The same procedure was followed for other Sn (0.04, 0.06, 0.08, and 0.1 M) concentrations. Ultimately, the synthesized nanoparticles can be collected for further characterization. For the Synthesis of pure ZnS nanoparticles the following procedure was employed. At first dissolving 0.1 M of zinc (II) acetate dihydrate in 100 ml of ethylene glycol. Stir this solution at room temperature for 30 minutes. Dissolve 0.3 M of thiourea in a separate container of 100 ml of ethylene glycol at ambient temperature. Gradually incorporate the thiourea solution into the existing solution containing zinc, ensuring continuous agitation and the same above mentioned procedure was followed.

## 3. PHOTOCATALYTIC ACTIVITY

The photocatalytic process using synthesized Sn alloyed ZnS nanostructures to degrade malachite green (MG) dye in water under UV irradiation in the air was studied. Initially, they dissolved 10 parts per million (ppm) of MB dye in 1000 millilitres of deionised water. They used a magnetic stirrer for 30 minutes to get a completely dissolved solution. A solution in which the dye is fully dissolved in deionised water is referred to as a stock solution. A 30 mg catalyst was added to a 50 ml stock solution. The mixture was then agitated constantly for 10 minutes and stored in a dark area. The graph was plotted at the wavelength of the MG dye at 617 nm. Subsequently, the solution underwent UV irradiation at various time intervals. Subsequently, UV absorption measurements were conducted at 30-minute intervals to monitor the breakdown of the dye. The decolourization demonstrates the photo-catalytic capability of $Zn_{1-x}Sn_xS$ nanoparticles. The determination of degradation efficiency can be achieved using the formula provided below:

$$\text{Degradation } (\%) = \frac{(A_0 - A_T)}{A_0} \times 100\% \qquad (1)$$

The absorbance values of the dye solution before UV irradiation are denoted as $A_0$, and the absorbance values of the dye solution after UV irradiation are denoted as $A_T$.

## 4. RESULTS AND DISCUSSION

### 4.1. Structural Analysis

The XRD patterns of both unalloyed and Zn-alloyed ZnS nanoparticles were examined, revealing a high level of crystalline quality. SnS nanoparticles have a maximum peak in (2θ = 28.367°) (JCPDS: 89-2755), and ZnS nanoparticles have a maximum peak in (2θ = 28.587°) (JCPDS file no. 65-5476). From the obtained X-ray Spectra we revealed that the synthesized nanoparticles are belongs to cubic crystal structure. As the concentration of Sn increases from 0.02 to 0.10 M, the dominant peak (1 1 1) continuously shifted towards the lower angle side. This peak shift confirming the formation of alloyed structure rather than formation of composites or separate nucleation of ZnS or SnS. (Jasrotia *et al*. 2022). The absence of any additional impurity diffraction peaks upon introducing the Sn into the ZnS lattices confirms the formation of a single-phase in both unalloyed and Sn-alloyed ZnS nanoparticles. As the amount of Sn increases in the parent ZnS lattices, other dominant peaks become less intense and continuously shifted towards the lower angle side. The Gaussian-fitted peaks for the (111) planes clearly show a slight shift in the peak position, confirming the successful alloying of Sn with ZnS nanoparticles. This shift, along with the intensity variation observed with increasing Sn incorporation from 0.02 to 0.10 M, is presented in Figure 1(b), further supporting the incorporation of Sn into the ZnS lattice.

The Scherer formula offers a method for determining the sizes of crystallites based on the FWHM of diffraction peaks. Crystallite sizes were found to be in the range from 25 to 50 nm. The lattice constant (a) varies depending on the Sn concentration, and their values are given in table 1. The lattice constant for the synthesized cubic crystal phase of pure ZnS and Sn alloyed ZnS nanoparticles are calculated using the following formula.

$$\frac{1}{d^2(\mathrm{hkl})} = \left(\frac{h^2+k^2+l^2}{a^2}\right) \qquad (2)$$

Where $d_{(hkl)}$ is the interplanar distance (nm).With the help of the W-H plot (Fig. 1(c)), it is possible to make estimations regarding the lattice parameters of Sn alloyed ZnS nanoparticles. The values of the lattice strain, derived from the W-H plots and provided in table 1, show that the strains are extremely minute. The random variation of micro strain values with increasing Sn concentration in ZnS observed in the Williamson-Hall (W-H) plot can be attributed to several factors. The incorporation of Sn into the ZnS lattice causes lattice distortion due to the size difference between $Zn^{2+}$ and Sn ions, leading to strain. However, non-uniform substitution, the possible formation of secondary phases or Sn-rich clusters, and the introduction of crystal defects can cause irregular changes in strain. These factors together lead to the observed random fluctuations in micro strain with varying Sn concentrations (Kumar *et al*. 2019). The change in crystallite size was observed as the concentration of Sn increased, as indicated by both the W-H method and Scherer's equation. The crystallite size and the unit cell properties have been influenced by the doping concentration of Sn (Chandrasekar *et al*. 2024).

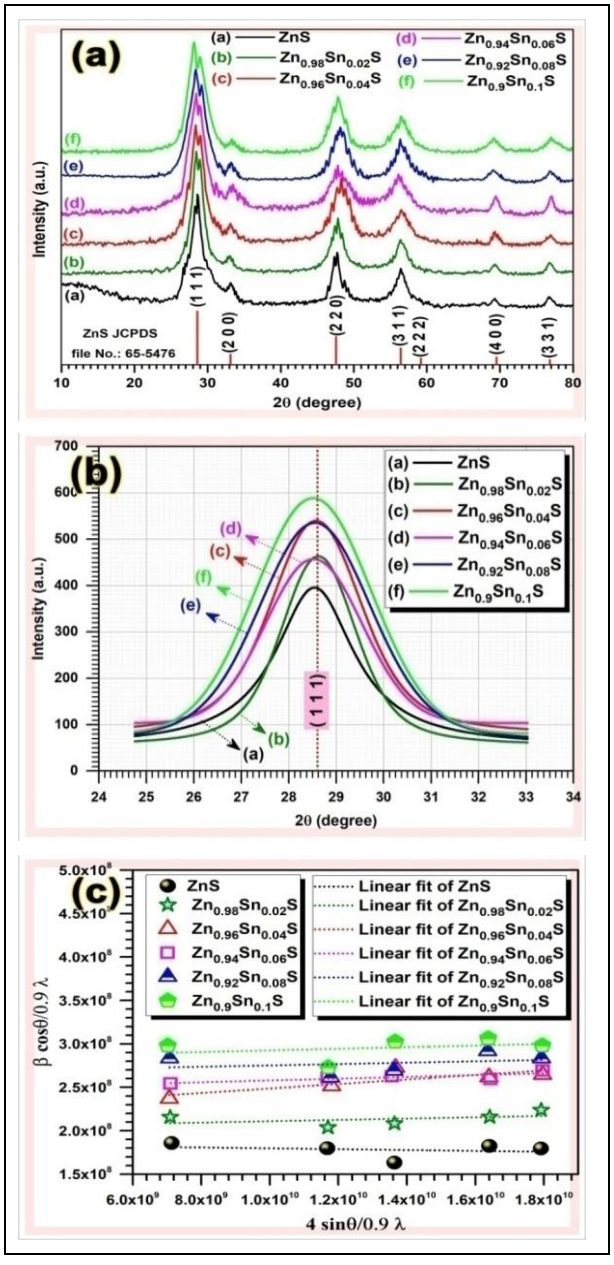


**Fig. 1: (a) XRD patterns of $Zn_{1-x}Sn_xS$ (x=0, 0.02, 0.04, 0.06, 0.08, 0.1 M) nanoparticles. (b) Gaussian peaks fitted to the (1 1 1) plane for $Zn_{1-x}Sn_xS$ (x=0, 0.02, 0.04, 0.06, 0.08, 0.1 M) nanoparticles. (c) W-H plots for $Zn_{1-x}Sn_xS$ (x=0, 0.02, 0.04, 0.06, 0.08, 0.1 M) nanoparticles**

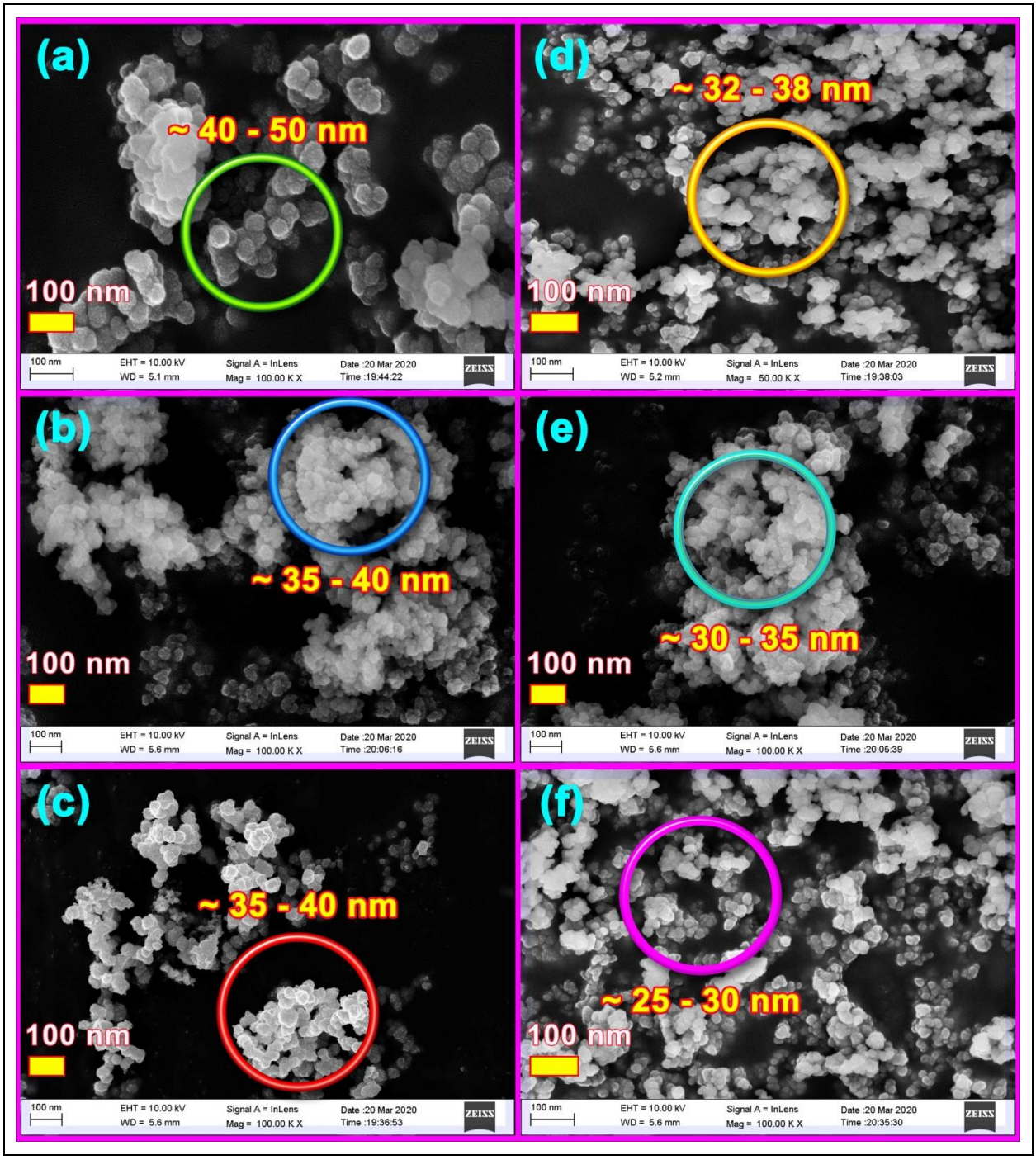


**Fig. 2: FESEM images of (a) ZnS, (b) $Zn_{0.98}Sn_{0.02}S$, (c) $Zn_{0.96}Sn_{0.04}S$, (d) $Zn_{0.94}Sn_{0.06}S$, (e) $Zn_{0.92}Sn_{0.08}S$, (f) $Zn_{0.9}Sn_{0.1}S$ nanoparticles**

Fig. 2 depicts FESEM images of $Zn_{1-x}Sn_xS$ (x = 0, 0.02, 0.04, 0.06, 0.08 and 0.1M) nanoparticles. The FESEM images indicate that $Zn_{1-x}Sn_xS$ nanoparticles exhibit excellent dispersion with a narrow size distribution and a spherical shape. The uniform distribution of nanoparticles enables an accurate determination of the particle diameter. With increased Sn concentration, the nanoparticles' size decreases from 50 nm to 25 nm. Sn concentration at 2% reported particle size is 35-40 nm. For 10% Sn concentration, particle size varies from 25-30nm. Overall, the ZnSnS nanoparticle size changed by 60- 62% due to the change in the Sn concentration.

## 4.2 Elemental Analysis

Fig. 3 depicts High-Resolution Transmission Electron Microscopy (HRTEM) images and Selected Area Electron Diffraction (SEAD) patternsfor (a) ZnS, (b)$Zn_{0.98}Sn_{0.02}S$, (c) $Zn_{0.94}Sn_{0.06}S$, (d) $Zn_{0.9}Sn_{0.1}S$ nanoparticles. $Zn_{1-x}Sn_xS$ nanoparticles in the HRTEM microstructure are evenly distributed and have a uniform

spherical shape with a narrow size range. The crystallite size of the (a) pure ZnS nanoparticle is 5.6 nm, and (b) $Zn_{0.98}Sn_{0.02}S$, (c) $Zn_{0.94}Sn_{0.06}S$, (d) $Zn_{0.9}Sn_{0.1}S$ nanoparticles, is 4.7 nm, 3.9 nm, and 3.6 nm, respectively. As the Sn concentration increases, the crystallite size from HRTEM micrographs decreases. The calculated crystallite size values align well with the values from the XRD data. The (111), (2 2 0), and (3 1 1) lattice planes of Cubic ZnS are represented by the diffraction rings observed in the SAED pattern, and these results align well with the findings of the XRD analysis. Measurement of the interplanar distance (d) is also carried out based on the SAED patterns. These findings agree with the X-ray diffraction (XRD) results. It revealed that the Sn alloyed ZnS nanoparticles were synthesized successfully using the SMI technique. An effective analytical method called Energy Dispersive X-ray Spectroscopy (EDAX) is utilized to qualitatively and quantitatively analyze the elemental composition of materials. EDAX analysis is commonly integrated with scanning electron microscopy (SEM) to provide information about the sample's elemental composition at specific points or areas of interest. Here's an overview of how EDAX analysis works.

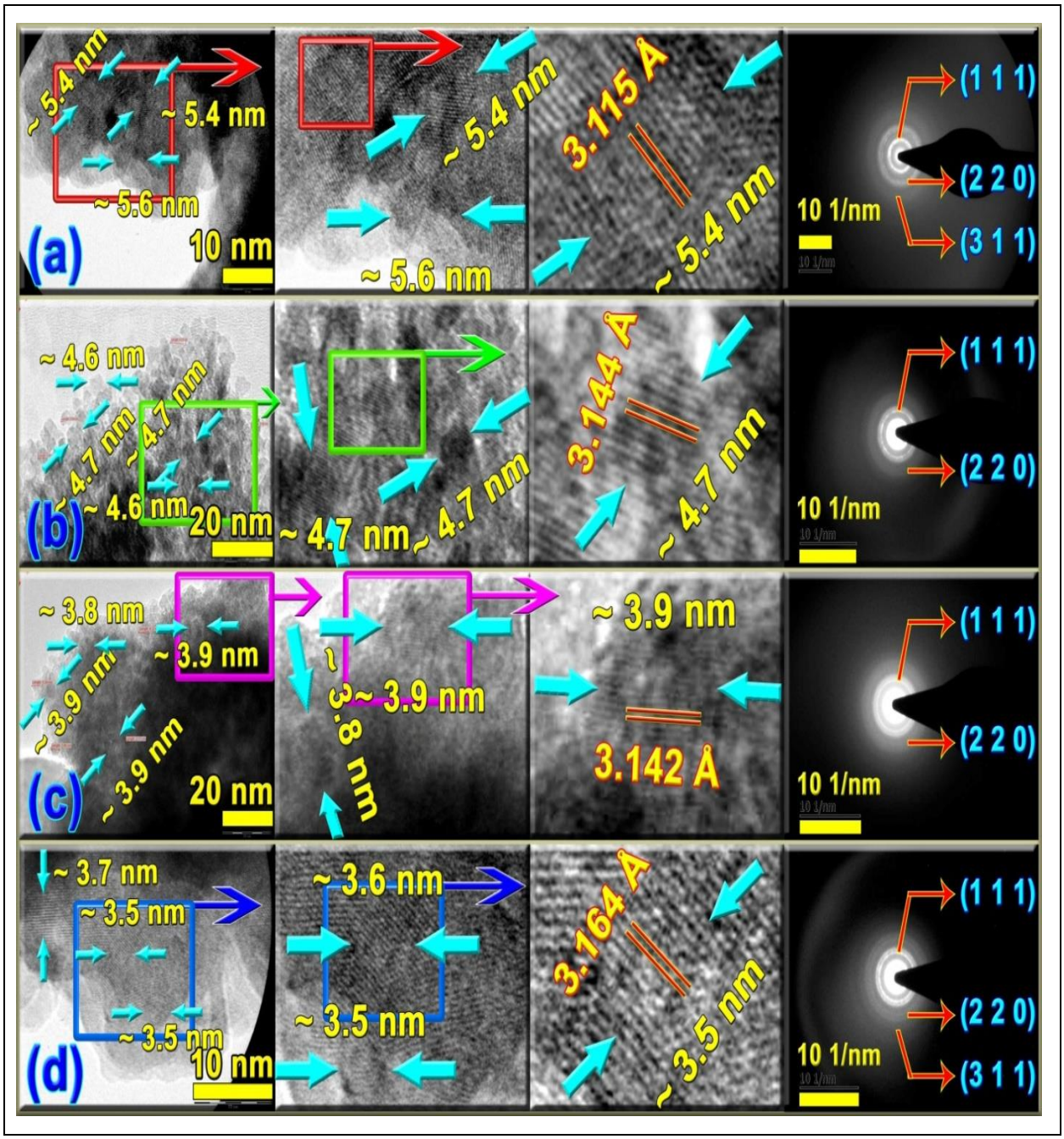


**Fig. 3: High-Resolution Transmission Electron Microscopy images and Selected Area Electron Diffraction patterns for (a) ZnS (b)$Zn_{0.98}Sn_{0.02}S$, (c) $Zn_{0.94}Sn_{0.06}S$, (d) $Zn_{0.9}Sn_{0.1}S$ nanoparticles**

Fig. 4 shows the EDAX spectrum of (a) ZnS, (b) $Zn_{0.98}Sn_{0.02}S$, (c) $Zn_{0.96}Sn_{0.04}S$, (d) $Zn_{0.94}Sn_{0.06}S$, (e) $Zn_{0.92}Sn_{0.08}S$, (f) $Zn_{0.9}Sn_{0.1}S$ nanoparticles. The EDAX analysis showed that all the sample elements (Zn, Sn, S) were in the expected stoichiometric ratio, and no additional elements were detected. The figure provides the elemental atomic weight percentage values. The EDAX analysis confirmed the purity of the samples.

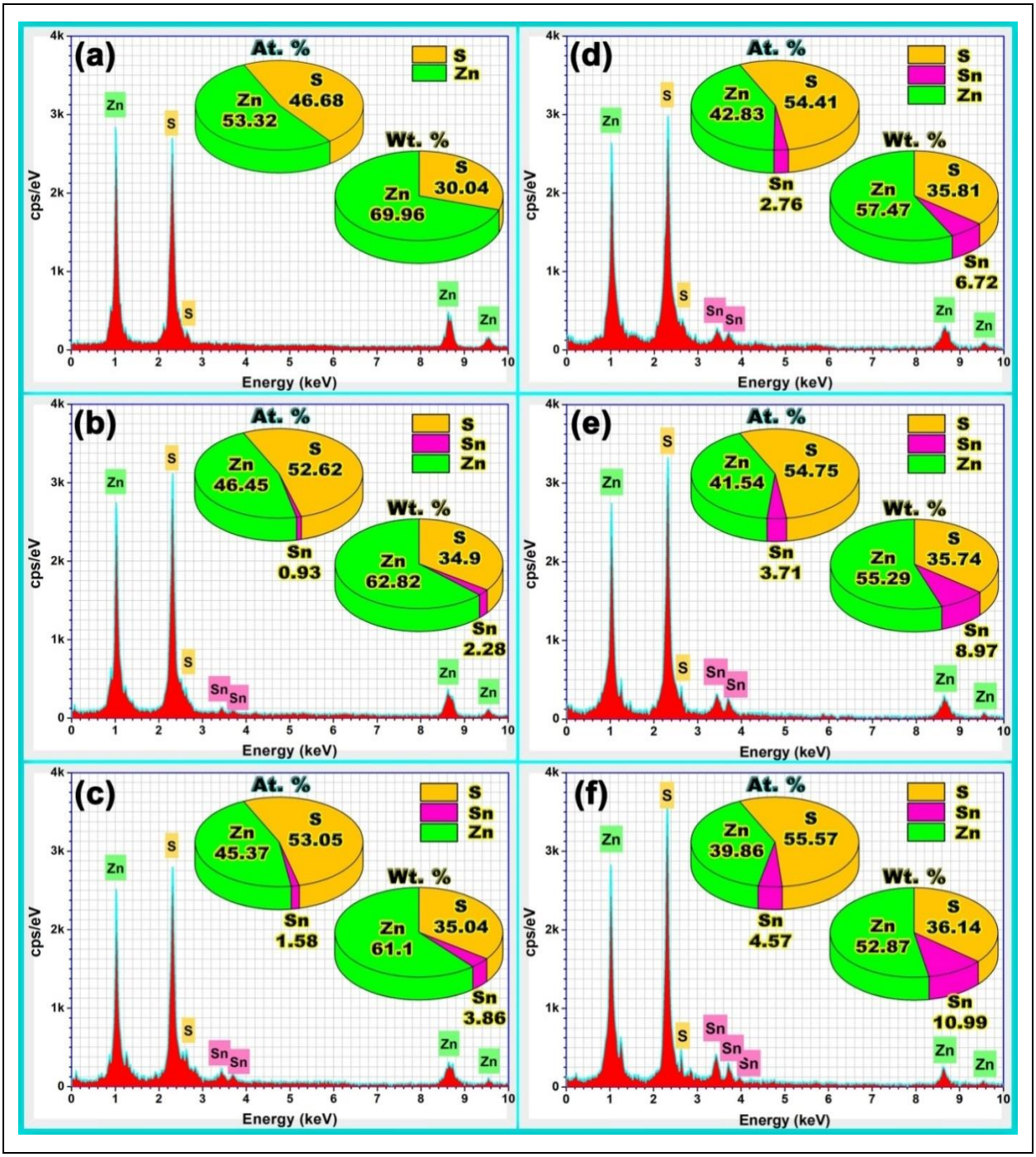


**Fig. 4: EDAX spectrum of (a) ZnS,(b) $Zn_{0.98}Sn_{0.02}S$, (c) $Zn_{0.96}Sn_{0.04}S$, (d) $Zn_{0.94}Sn_{0.06}S$, (e) $Zn_{0.92}Sn_{0.08}S$, (f) $Zn_{0.9}Sn_{0.1}S$ nanoparticles**

## 4.3 Optical Study

Fig. 5 depicts the UV absorption spectra of ZnS, $Zn_{0.98}Sn_{0.02}S$, $Zn_{0.96}Sn_{0.04}S$, $Zn_{0.94}Sn_{0.06}S$, $Zn_{0.92}Sn_{0.08}S$, $Zn_{0.9}Sn_{0.1}$ Snanoparticles. The unalloyed and Sn alloyed ZnS nanoparticles exhibit shorter wavelength tail bands in their absorption spectra, indicating a narrow and uniform particle size distribution (Abd *et al.*2010). It is evident from the spectra that the absorption peak intensifies as the concentration of Sn increases. The bandgap energy ($E_g$) values for Sn alloyed ZnS nanoparticles were determined from the Tauc plot and are

given table 2. By changing to a high value, the concentration of Sn, the bandgap changed to a low value, because the Fermi energy level overlaps with the conduction band. This particular property of Sn-alloyed ZnS nanomaterials holds significant potential for various applications across multiple fields, such as optoelectronic devices, sensors, and as an efficient photocatalyst (Shah *et al*. 2023; Gedi*et al*. 2016; Sebastian *et al*. 2020; Kunapalli*et al*. 2022).

**Table 1. The calculated structural data of $Zn_{1-x}Sn_xS$ (where x = 0, 0.02, 0.04, 0.06, 0.08 and 0.1) nanoparticles from powder XRD spectra**

| Sample Name | Peak Position (deg) | a (Å) | Crystallite Size (nm) | | Micro Strain ($x10^{-3}$) |
|---|---|---|---|---|---|
| | | | W-H Method | Scherer Formula | |
| ZnS | 28.562 | 5.402 | 18.72 | 18.64 | -2.142 |
| $Zn_{0.98}Sn_{0.02}S$ | 28.548 | 5.411 | 17.23 | 17.45 | -1.807 |
| $Zn_{0.96}Sn_{0.04}S$ | 28.521 | 5.413 | 16.41 | 17.09 | 3.670 |
| $Zn_{0.94}Sn_{0.06}S$ | 28.519 | 5.406 | 15.72 | 15.63 | 1.571 |
| $Zn_{0.92}Sn_{0.08}S$ | 28.502 | 5.404 | 15.13 | 14.91 | 1.203 |
| $Zn_{0.9}Sn_{0.1}S$ | 28.490 | 5.410 | 14.35 | 14.16 | 0.812 |

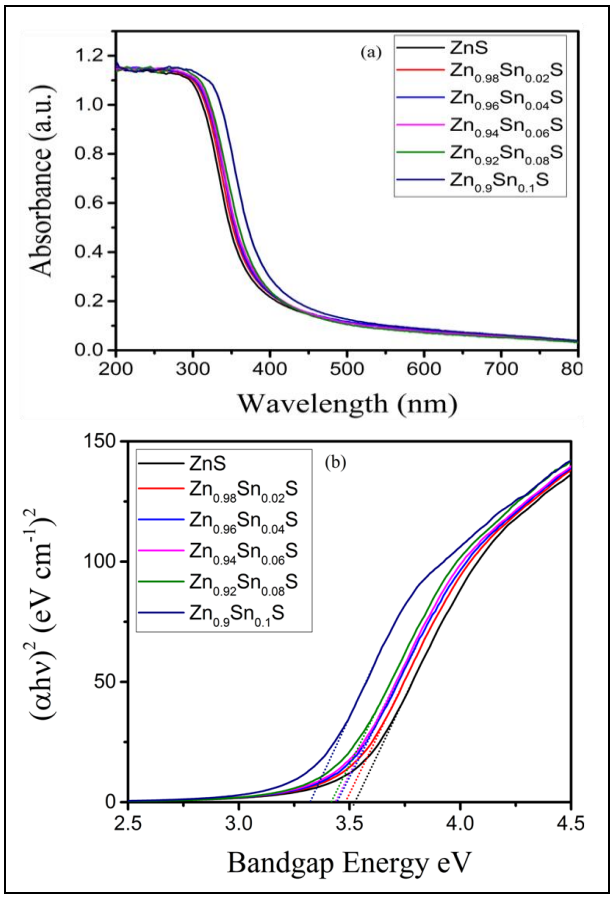


**Fig. 5: (a) UV spectra-$Zn_{1-x}Sn_xS$ (x=0,0.02,0.04,0.06,0.08,0.1) nanoparticles.b) Graph poltted for Bandgap energy of $Zn_{1-x}Sn_xS$ (x=0,0.02,0.04,0.06,0.08,0.1)nanoparticles**

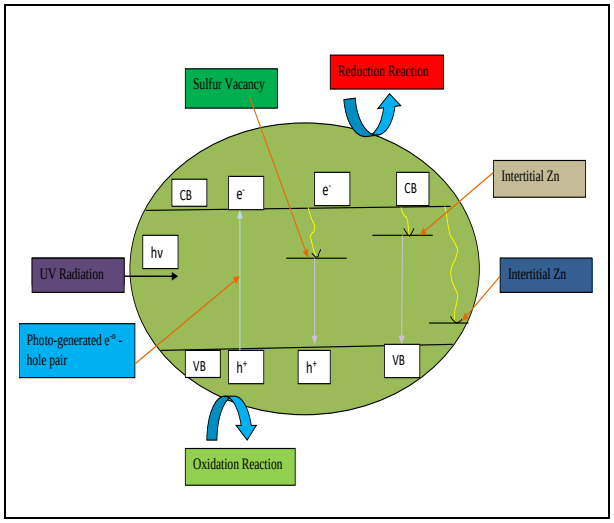


**Fig.6: Schematic representation of various process involved in Photocatalytic activity**

**Table 2. Bandgap energy $E_g$ for the ZnS, $Zn_{0.98}Sn_{0.02}S$, $Zn_{0.96}Sn_{0.04}S$, $Zn_{0.94}Sn_{0.06}S$, $Zn_{0.92}Sn_{0.08}S$, $Zn_{0.9}Sn_{0.1}S$ nanoparticles from Tauc plot**

| Sample | Bandgap energy $E_g$ in eV |
|---|---|
| ZnS | 3.52 |
| $Zn_{0.98}Sn_{0.02}S$ | 3.49 |
| $Zn_{0.96}Sn_{0.04}S$ | 3.46 |
| $Zn_{0.94}Sn_{0.06}S$ | 3.45 |
| $Zn_{0.92}Sn_{0.08}S$ | 3.41 |
| $Zn_{0.9}Sn_{0.1}S$ | 3.31 |

Equation (3) relate absorption co-efficient with incident photon energy such as

$$\alpha h\nu = A(h\nu - E_g)^m \qquad (3)$$

Where h, ν, $E_g$and m is the plank constant, photo frequency, bandgap, and index indicating the type of transition, respectively. The value of m is ½ for the direct bandgap, and for the indirect bandgap is 2. Increasing the Sn concentration minimised bandgap energy $E_g$ for Sn alloyed ZnS nanoparticles (Asfiaand Rashid, 2022; Ramki *et al*.2022). From XRD, crystallite size decreases when the Sn concentration is increased, which leads to a decrease in the bandgap energy $E_g$ of nanoparticles.

## 4.4 Photocatalytic Study

### 4.4.1 Photocatalytic Mechanism

Wavelength between 500 and 700 nm shows the absorption spectrum for visible light. These wavelengths are within the range of light that is visible to humans. In absorption spectra, this range typically indicates light absorption by specific substances within the visible spectrum. Light absorption within this range is linked to

electronic transitions in molecules or materials (Ramki *et al.*2020). The photocatalytic reaction process (Fig. 6) can be described as follows:

$$ZnS/SnS + h\nu\ (UV/\ Solar\ radiation) \rightarrow e^- + h^+$$

The oxidation of water by holes $[H_2O] \leftrightarrow H^+ + OH$

$$h^+ + H_2O \rightarrow OH^*$$

$$O_2 + e^- \rightarrow O_2^{-*}$$

The transient formation of hydro peroxide radicals:

$$2H_2O + e^- + O_2^{-*} \rightarrow 2OH^* + 2OH^-$$

Reaction between a reactive intermediate and dye molecules is tentatively undergoing degradation.

$OH^* + O_2^{-*}$ + MG dye → Degradable/less-toxic species

#### 4.4.2 Impact of a catalyst on the degradation of Malachite Green dye (MG)

The changes in the colour of a malachite green (MG) dye solution with both pure ZnS and Sn-alloyed ZnS nanoparticles after UV radiation exposure are shown in the absorption spectra in Fig. 7 at different time intervals (0 to 120 minutes). The UV absorption wavelength of Malachite green dye is 617 nm (Shirmardi *et al.*2013). The intensity of the peaks changed to low as a result of UV radiation-induced degradation of the MG dye solution. As the dopant concentration increases, the degradation efficiency also increases. The efficiency of degradation increases from 51% to 69% with the increase in Sn concentration.

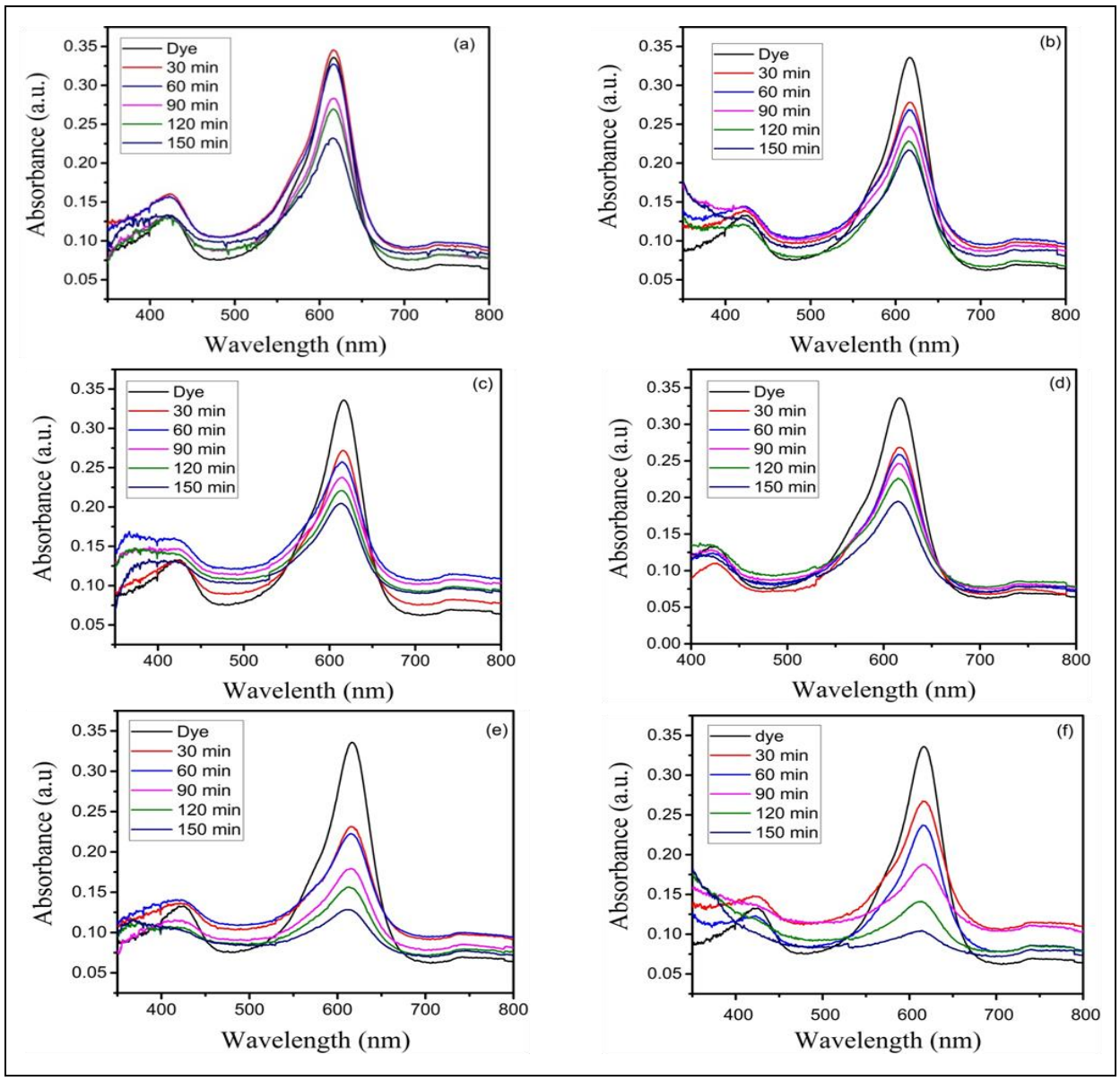


**Fig.7: Depict the colour changes in a malachite green (MG) dye solution containing (a) ZnS and (b) $Zn_{0.98}Sn_{0.02}S$, (c) $Zn_{0.96}Sn_{0.04}S$, (d) $Zn_{0.94}Sn_{0.06}S$, (e) $Zn_{0.92}Sn_{0.08}S$, (f) $Zn_{0.9}Sn_{0.1}S$ nanoparticles at various time (0 to 150 minutes) intervals**

## 5. CONCLUSION

Pure and Sn alloyed ZnS nanoparticles were successfully synthesized using the simple SMI technique. XRD study reveals that the pure ZnS, $Zn_{0.98}Sn_{0.02}S$, $Zn_{0.96}Sn_{0.04}S$, $Zn_{0.94}Sn_{0.06}S$, $Zn_{0.92}Sn_{0.08}S$, $Zn_{0.9}Sn_{0.1}Sn$ anoparticles have formed cubic structure confirmed by suitable JCPDS file- the nanoparticle's crystallite size changes when the Sn concentration increases. The cubic crystal structure's presence slightly shifted towards the lower angle side due to the overlapping of ZnS with SnS, which confirmed alloy formation. FESEM and HRTEM studies revealed that $Zn_{1-x}Sn_x$ Snanoparticles are well dispersed with a narrow size distribution, and spherical and crystallite sizes of the nanoparticles were calculated. Crystallite size values $Zn_{1-x}Sn_xS$ nanoparticles match well with the XRD data.EDAX characterization study confirms the presence of all elements and chemical purity in the synthesized crystal of $Zn_{1-x}Sn_xS$ nanoparticles. The bandgap energy value changed from 3.52eV to 3.31eV. Due to its wide range of properties, the formation of tin-alloyed zinc sulfide nanoparticles in this material offers various applications in electronics, energy conversion, and catalysis. Tested photocatalytic activity of $Zn_{1-x}Sn_xS$ nanoparticles on malachite green dye (MG) shows 51-69% degradation efficiency. As we control, recombining the electron-hole pair with the suitable capping agent will increase the degradation efficiency of Sn alloyed ZnS.

## ACKNOWLEDGEMENTS

The authors thankful to the Cochin University of Science and Technology, PSG Institute of Technology, Coimbatore, for their assistance with characterization studies. The authors extend their heartfelt thanks to Mrs. T. Shobana, Research Scholar, Department of Physics, Chikkanna Government Arts College, Tiruppur, for valuable discussions.

## FUNDING

There is no funding source.

## CONFLICT OF INTEREST

The authors declared no conflict of interest in this manuscript regarding publication.

## COPYRIGHT



## REFERENCE

Abd, E. M. S. and Babu, S. M., Growth and optical characterization of colloidal CdTe nanoparticles capped by a bifunctional molecule, *Physica B*, 405(16), 3279-3283 (2010). https://doi.org/10.1016/j.physb.2010.04.060

Asfia, M. B. and Rashid, M. A., First principles calculations of structural, electronic and optical properties of Sn-alloyed ZnS, *Physica B*, 646, 414335 (2022). https://doi.org/10.1016/j.physb.2022.414335

Gedi, S., Reddy, V. R. M., Kotte, T. R. R. and Kim, S. H., Jeon, C. W., "Chemically synthesized Ag-alloyed ZnS films for PV applications, *Ceram. Int.*, *42*(16), 19027-19035 (2016). https://doi.org/10.1016/j.ceramint.2016.09.059

Chandrasekar, L. B., Gnaneswari, M. D., Murugeswari, A., Sundaram, P. S., Ananthan, N., & Karunakaran, M., Preparation, characterization, and antibacterial activity of Ni, Sn co-doped ZnO nanoparticles: Effect of Sn doping concentration., Journal of Crystal Growth., 633, 127660 (2024). https://doi.org/10.1016/j.jcrysgro.2024.127660

Gowdhaman, P., Praveen, V. N., Saravanan, R. S. S., Venkateswari, P. and Pandya, H. M., Facile synthesis of undoped and Sn doped CdS nanoparticles for dye-sensitized solar cell applications, *Opt. Mater.*, 120, 111465 (2021). https://doi.org/10.1016/j.optmat.2021.111465

Gowdhaman, P., Sakthi SudarSaravanan, R., Venkatesan, T. and Haresh M. Pandya, Wide Bandgap Semiconductor Alloy Nanomaterials for Potential Applications – A Future Perspective Approach, *J. Environ. Nanotechnol.*, 7(1), 37-40 (2018). https://dx.doi.org/10.13074/jent.2018.03.181299

Hammad, T. M., Salem, J. K., Kuhn, S., Draaz, M. A., Hempelmann, R. and Kodeh, F. S., Optical properties of $Cu^{2+}$ and $Fe^{2+}$ doped ZnS semiconductor nanoparticles synthesized by co-precipitation method, *J. Mater. Sci.: Mater. Electron.*, 26, 5495-5501 (2015). https://doi.org/10.1007/s10854-015-3106-0

Jasrotia, R., Verma, A., Verma, R., Godara, S. K., Ahmed, J., Mehtab, A. and Kalia, S., Photocatalytic degradation of malachite green pollutant using novel dysprosium modified Zn–Mg photocatalysts for wastewater remediation, *Ceram. Int.*, 48(19), 29111-29120 (2022). https://doi.org/10.1016/j.ceramint.2022.05.050

Juan, J. R. M., Levchuk, I., Ibañez, P. F. and Sillanpää, M., A critical review on application of photocatalysis for toxicity reduction of real wastewaters, *J. Cleaner Prod.*, 258, 120694 (2020).

Kumar, R., Sakthivel, P., & Mani, P., Structural, optical, electrochemical, and antibacterial features of ZnS nanoparticles: incorporation of Sn. Applied Physics A, 125(8), 543 (2019). https://doi.org/10.1016/j.jclepro.2020.120694

Kripal, R., Gupta, A. K., Mishra, S. K., Srivastava, R. K., Pandey, A. C. and Prakash, S. G., Photoluminescence and photoconductivity of ZnS: Mn2+ nanoparticles synthesized via co-precipitation method, *Spectrochim. Acta, Part A*, 76(5), 523-530 (2010). https://doi.org/10.1016/j.saa.2010.04.018

Kunapalli, C. K., Chakraborty, D. and Shaik, K., Structural, optical, and magnetic properties of Sn-alloyed ZnS thin films: role of post-annealing, J. Aust. Ceram. Soc., 58(4), 1105-1110 (2022). https://doi.org/10.1007/s41779-022-00786-3

Mehra, S., Singh, M. and Chadha, P., Adverse impact of textile dyes on the aquatic environment as well as on human beings, *Toxicol. Int*., 28(2), 165 (2021). https://doi.org/10.18311/ti/2021/v28i2/26798

Nasrollahzadeh, M., Sajadi, S. M., Sajjadi, M., Issaabadi, Z., An introduction to nanotechnology, *Interface Sci. Technol*., 28, 1-27 (2019). https://doi.org/10.1016/B978-0-12-813586-0.00001-8

Rajabi, H. R. and Farsi, M., Effect of transition metal ion doping on the photocatalytic activity of ZnS quantum dots: synthesis, characterization, and application for dye decolorization, *J. Mol. Catal. A: Chem.* , 399, 53-61 (2015). https://doi.org/10.1016/j.molcata.2015.01.029

Ramki, K., Raja, P. A., Sakthivel, P., Murugadoss, G., Thangamuthu, R. and Rajesh, K. M., Rapid degradation of organic dyes under sunlight using tin-alloyed ZnS nanoparticles, *J. Mater. Sci.: Mater. Electron.*, 31, 8750-8760 (2020). https://doi.org/10.1007/s10854-020-03410-x

Sabaghi, V., Davar, F. and Fereshteh, Z., ZnS nanoparticles prepared via simple reflux and hydrothermal method: Optical and photocatalytic properties, *Ceram. Int*., 44(7), 7545-7556 (2018). https://doi.org/10.1016/j.ceramint.2018.01.159

Saravanan, R. S. S. and Mahadevan, C. K., Photoluminescence and electrical impedance measurements on alloyed Zn (1− x) CdxS nanocrystals, *J. Alloys Compd.*, 541, 115-124 (2012). https://doi.org/10.1016/j.jallcom.2012.06.048

Sonawane, J. R., & Kulkarni, A. A., Model predicted optimization of experimental set-up and process conditions for microwave-assisted synthesis of silver nanowires. Chemical Engineering Journal, 155483 (2024). https://doi.org/10.1016/j.cej.2024.155483

Sebastian, S., Kulandaisamy, I., Valanarasu, S., Yahia, I. S., Kim, H. S. and Vikraman, D., Microstructural and electrical properties evaluation of lead alloyed tin sulfide thin films, *Journal of Sol-Gel Science and Technology*, 93, 52-61 (2020). https://doi.org/10.1007/s10971-019-05169-y

Shah, U., Jan, F. A., Ullah, R., Wajidullah, Ullah, N. and Ahmad, M., Photocatalytic Degradation of Acidic and Basic Dye by ZnS and Tin-Alloyed ZnS Nanocatalysts, *Iran. J. Sci.*, 47(3), 733-747 (2023). https://doi.org/10.1007/s40995-023-01462-2

Sharma, K., Raizada, P., Hasija, V., Singh, P., Bajpai, A., Nguyen, V. H. and Van, L., Q., ZnS-based quantum dots as photocatalysts for water purification, *J. Water Process Eng*., 43, 102217, (2021). https://doi.org/10.1016/j.jwpe.2021.102217

Shirmardi, M., Mahvi, A. H., Hashemzadeh, B., Naeimabadi, A., Hassani, G., & Niri, M. V.,The adsorption of malachite green (MG) as a cationic dye onto functionalized multi walled carbon nanotubes. Korean Journal of Chemical Engineering, 30, 1603-1608(2013). https://doi.org/10.1007/s11814-013-0080-1

Tong, Y., Hou, Y., Zhang, Z., Yan, L., Chen, X., Zhang, H. and Li, Y., Current progress of metal sulfides derived from MOFs for photocatalytic hydrogen evolution, *Appl. Catal., A*, 119387, (2023). https://doi.org/10.1016/j.apcata.2023.119387

Velumani, S. and Ascencio, J. A., Formation of ZnS nanorods by simple evaporation technique, *Appl. Phys. A*, 79, 153-156, (2004). https://doi.org/10.1007/s00339-003-2367-2

Xu, X., Li, S., Chen, J., Cai, S., Long, Z., Fang, X., Design principles and material engineering of ZnS for optoelectronic devices and catalysis, *Adv. Funct. Mater*., 28(36), 1802029 (2018). https://doi.org/10.1002/adfm.201802029

Yin, L., Wang, D., Huang, J., Cao, L., Ouyang, H. and Yong, X., Morphology-controllable synthesis and enhanced photocatalytic activity of ZnS nanoparticles, *J. Alloys Compd*., 664, 476-480 (2016). https://doi.org/10.1016/j.jallcom.2015.10.281

Zhou, M., Gong, Y., Xu, J., Fang, G., Xu, Q. and Dong, J., Colloidal CZTS nanoparticles and films: preparation and characterization, *J. Alloys Compd*., 574, 272-277 (2013) https://doi.org/10.1016/j.jallcom.2013.05.143